

Sliding Mode and Continuous Estimation Techniques for the Realization of Advanced Control Strategies for Parallel Kinematics

S. Flottmeier * S. Olma * A. Trächtler *

* *Heinz Nixdorf Institute, University of Paderborn, Fürstenallee 11,
33102 Paderborn, Germany (e-mail: {sarah.flottmeier, simon.olma,
ansgar.traechtler}@hni.upb.de).*

Abstract: The realization of advanced control concepts for parallel kinematic machines (PKM) requires the knowledge of system states. Despite the fact that the direct kinematic problem (DKP) is not explicitly solvable for PKMs they need not to be measured directly. This can be achieved by the usage of state estimation techniques, which can also be extended for disturbance estimation and hence allow for disturbance compensation - a possibility that direct measurement devices or iterative algorithms to solve the DKP cannot provide for. Subsequently, two possibilities for the realization of adequate estimation are presented: a new approach for the state and disturbance estimation for PKMs via sliding mode techniques and a more classical approach based on continuous Kalman filtering. Their suitability for the usage within an advanced state control scheme is validated simulatively with models of different complexity of a hydraulically actuated hexapod intended to be used as a motion simulator for automotive testing purposes.

Keywords: robotics; sliding mode; state estimation; disturbance estimation; state feedback; nonlinear systems.

1. INTRODUCTION

In comparison to serial kinematic structures, parallel kinematic machines (PKMs) are advantageous for applications with testing purposes. They have small moving masses leading to a great potential for the realization of dynamic excitations in different mechanical degrees of freedoms (DOF). However, the exploitation of this potential requires advanced control strategies considering the structural specialties in a model based control approach. Here, control schemes in global Cartesian coordinates can assumed to be more suitable compared to the ones in joint space coordinates, as many authors, e.g. Merlet [2002] and Paccot et al. [2009], agree. Despite this, mostly controls in joint space coordinates are used in real applications, because joint space measurement data can be obtained more easily.

Paccot et al. [2009] name two possibilities for the direct measurement of the global Cartesian end effector position of PKMs: camera and laser based methods. However, the authors point out that these optical measurement devices are cost intensive and/or hard to implement and have not been applied for the usage within advanced dynamic control systems, yet. An intuitive approach to cope with this difficulty is the calculation of the needed feedback data in global Cartesian coordinates from the available joint space measurement data. But the correlation between joint space and Cartesian coordinates, the so-called direct kinematic problem (DKP), generally cannot be formulated explicitly for PKMs, see Merlet [2006]. Hence, this forms

a challenge that needs to be tackled for the realization of control schemes in global Cartesian coordinates.

For the solution of the DKP for PKMs the usage of iterative algorithms is well established, e.g. different methods can be found in Merlet [2006]. However, Abdellatif et al. [2008] point out that the suitability of iterative solutions is limited for control purposes, especially, if velocity feedback is needed, too. This is computed from the iterative solution by differentiation and has to be filtered because of the resulting noise level. This leads to phase delay and hence results in the limitation of the reachable bandwidth for the closed control loop.

Further approaches consist of the application of estimation techniques, which has been proposed by several authors to overcome the above mentioned realization problems. The suggested methods can basically be divided into discontinuous and continuous approaches. One of the latter is described by Chen et al. [2013], where the application of a nonlinear observer to solve the DKP for a six DOF Stewart platform, is presented. There, the concept is to apply a nonlinear state transformation by the calculation of Lie derivatives to transform the system in a linear description. Afterwards the design of the observer gain matrix can be performed easily. In Kang et al. [1998] a nonlinear robust estimator, which considers nonlinearity and uncertainty in the system, is proposed. The authors analyze and prove the observer stability with a Lyapunov function. In Fraguera et al. [2012] the authors make use of sliding mode estimation techniques. They investigate high order sliding mode (HOSM) observers for state estimation

and unknown input identification for a Stewart platform with three DOF, while position measurement data of the upper platform is assumed to be available. To date, we are not aware of any applications of sliding mode observers to solve the DKP for a six DOF Stewart platform.

References for the application of more classical continuous estimation techniques applied for the solution of the DKP for PKMs are e.g. Fasse et al. [2000] or Flottmeier et al. [2013], where different Kalman filtering approaches are used. In Flottmeier et al. [2013] it is shown, that a nonlinear observer model can be used with a constant observer gain matrix for the state estimation of a six DOF Stewart platform, also called *hexapod*, despite the system's nonlinearities. This makes the observer easy to implement for realtime purposes.

The main issue of this article is the presentation of two approaches for the state and disturbance estimation, applicable within advanced motion control strategies for PKMs. For the realization of both approaches the measurement of joint space data, which in general can be easily obtained, is sufficient. First, in terms of discontinuous observation, we present a new hierarchical sliding mode observer approach. Basically, the proposed observer is based on the observer structure for controlled nonlinear systems with a single output from Drakunov et al. [2011]. Here, we present the applicability of the observer for nonlinear multiple input multiple output (MIMO) systems, e.g. PKMs. Secondly, in terms of more classical approaches, the continuous Kalman filter, which has been presented in Flottmeier et al. [2013], is extended for disturbance estimation. The feasibility of the proposed observers can be shown via various simulation results.

The article is structured as follows: Section 2 deals with the system model, Section 3 is dedicated to an advanced state control scheme for the motion control of PKMs. In Section 4 we present a new approach for sliding mode estimation and a more classical estimation approach based on Kalman filtering. In Section 5, simulation results are shown, which have been generated with a simple six DOF model and a complex multi body system (MBS) model of a hydraulically actuated hexapod to demonstrate and compare the effectiveness of the estimation approaches. The article ends with a short future outlook in Section 6.

2. SYSTEM MODEL

The target system consists of a hydraulically actuated hexapod, whose structure is pictured schematically in Fig. 1. It shall be used as a motion simulator for automotive testing purposes and is currently installed in the lab of the Heinz Nixdorf Institute at the University of Paderborn. In terms of control performance the goal is to achieve a bandwidth up to 80 Hz for the position controlled system for small amplitudes $< 1\text{ mm}$.

For the controller and observer design a system model is required. In this section, the state space model of the hexapod is described. The main system parameters are listed in Table 1, while the locations of the used coordinate systems are shown in Fig. 1. The fixed inertial Cartesian coordinate system N is located in the center of the base platform, whereas the moving coordinate system E is fixed

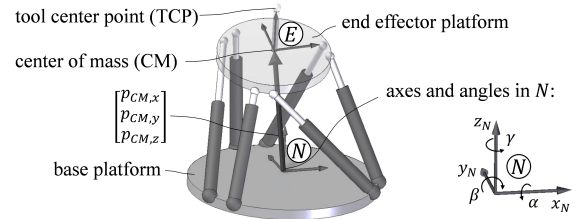


Fig. 1. Target system: Hexapod

to the end effector platform and located in its center of mass.

Table 1. System parameters

base platform radius	r_B	750 mm
end effector platform radius	r_E	450 mm
end effector platform mass	m_G	217 kg
minimum actuator length	l_{min}	785 mm
maximum actuator stroke	l_{max}	230 mm

The hexapod has six actuators and six DOF, hence six differential equations of second order can be derived to describe the dynamic motion of the end effector relative to N . These equations of motion can be formulated via the Lagrange formalism resulting in

$$M(x)\dot{v} + C(x, v)v + G = F_{act, N}. \quad (1)$$

Here, $M(x) \in \mathbb{R}^{6 \times 6}$ denotes the inertia matrix of the end effector. It depends on the current posture of the end effector, described by the position vector

$$x = [p_{CM, x} \ p_{CM, y} \ p_{CM, z} \ \alpha \ \beta \ \gamma]^T, \quad (2)$$

where $p_{CM, x}$, $p_{CM, y}$ and $p_{CM, z}$ are the x -, y - and z -coordinates of the center of mass in N and α , β and γ are the rotation angles of the coordinate system E with respect to N around its three axes in the x_N - y_N - z_N -sequence, respectively. The translational and rotational velocities of the center of mass of the end effector in N form the velocity vector

$$v = [v_{CM, x} \ v_{CM, y} \ v_{CM, z} \ \omega_x \ \omega_y \ \omega_z]^T. \quad (3)$$

The relation between the velocity vector v and the time derivatives of x is given by the kinematic matrix $H(x)$:

$$v = H(x) \cdot \dot{x}, \quad (4)$$

where $H(x)$ is defined as

$$H(x) = \frac{\partial v}{\partial \dot{x}}. \quad (5)$$

It can be calculated using the tilde matrix of angular velocities for the movement of E with respect to N , which is defined as follows (cf. Roberson et al. [1988], p. 81):

$${}^N \tilde{\omega}_{NE}(x, \dot{x}) = \begin{bmatrix} 0 & -\omega_z & \omega_y \\ \omega_z & 0 & -\omega_x \\ -\omega_y & \omega_x & 0 \end{bmatrix} = \dot{T}_{NE}(x, \dot{x}) \cdot T_{NE}^T(x). \quad (6)$$

Here, the rotation sequence is considered by the rotation matrix $T_{NE}(\alpha, \beta, \gamma)$, which can be used to transform arbitrary vectors from E , e.g. ${}^E r$, to N , e.g. ${}^N r = T_{NE} \cdot {}^E r$, and its time derivative $\dot{T}_{NE}(\alpha, \beta, \gamma, \dot{\alpha}, \dot{\beta}, \dot{\gamma})$.

The joint space coordinates $q_1 \dots q_6$ (lengths of the actuators) are collected in the vector

$$q = [q_1 \ \dots \ q_6]^T. \quad (7)$$

In contrast to the DKP, the relation between x and q can be formulated explicitly for PKMs. This is referred

to as the inverse kinematics problem (IKP) and can be expressed by the nonlinear function $q(x)$.

The velocity vector v is related to the time derivative \dot{q} of the joint coordinates via

$$v = J(x) \cdot \dot{q}, \quad (8)$$

where $J(x)$ denotes the Jacobian. Its inverse $J^{-1}(x)$ can be symbolically calculated via

$$J^{-1}(x) = \frac{\partial q(x)}{\partial x} \cdot H^{-1}(x). \quad (9)$$

For the target system, $J(x)$ can be obtained by inversion, as $J^{-1}(x)$ is regular for the entire effective workspace.

The vector $C(x, v)v \in \mathbb{R}^6$ contains the Coriolis- and centrifugal forces, whereas $G \in \mathbb{R}^6$ represents the vector of gravitational force. $F_{act, N} = [F_x F_y F_z M_x M_y M_z]^T$ denotes the vector of forces and torques in N , acting at the center of mass of the end effector. It results from the single actuator forces $F_{act} = [f_1 \dots f_6]^T$. They form the joint forces, whose relation to $F_{act, N}$ again is given by the Jacobian $J(x)$:

$$F_{act, N} = J^{-T}(x) \cdot F_{act}. \quad (10)$$

For control and observer design purposes a nonlinear state space representation of the equations of motion, cf. (1), is needed. In order to achieve this, the system can be formulated as a MIMO nonlinear control affine system as follows:

$$\dot{z} = f(z) + g(z)u \quad (11)$$

$$y = h(z), \quad (12)$$

where

$$z = [x^T v^T]^T, \quad (13)$$

$z \in \mathbb{R}^{12}$, denotes the state vector consisting of the global position coordinates x and the velocity vector v , and the input vector $u \in \mathbb{R}^6$ consists of the actuator forces

$$u = F_{act}. \quad (14)$$

The system output y is given by the measurable joint coordinates q :

$$y = q(x). \quad (15)$$

By means of (1)-(10), the state space equations, cf. (11)-(12), yield

$$f(z) = \begin{bmatrix} 0 & H^{-1}(x) \\ 0 & -M^{-1}(x)C(x, v) \end{bmatrix} z + \begin{bmatrix} 0 \\ -M^{-1}(x)G \end{bmatrix}, \quad (16)$$

$$g(z) = \begin{bmatrix} 0 \\ M^{-1}(x)J^{-T}(x) \end{bmatrix}, \quad (17)$$

$$h(z) = q(x). \quad (18)$$

3. ADVANCED STATE CONTROL STRATEGY

Common approaches for the control of PKM base on exact linearization techniques, where the nonlinear behavior of the target system is compensated for via online calculation of the inverse dynamics. As it can be seen from the section above, the current system states have to be known for this purpose. If they are used for linearization, it is referred to as *feedback linearization*, if the reference variables are used instead, as *feed forward linearization*, cf. Kolbus et al. [2010]. This can be applied for joint space control to avoid the necessity to solve the DKP. However, Kolbus

et al. [2010] also point out that the usage of feedback linearization and state control is advantageous in terms of decoupling, which is also confirmed by Paccot et al. [2009]. We also prefer the feedback linearization approach and suggest the usage of pole assignment techniques for the control design, whose major aspects for the usage within the motion control of six DOF PKMs are described subsequently.

For the application of pole assignment techniques, a full decoupling of the dynamic system behavior is required, resulting in a double integrative behavior for each mechanical DOF. This can be achieved by exact feedback linearization. In order to obtain adequate linearization terms, the equations of motion introduced in the previous section have to be modified to depend on x and its derivatives. This can be achieved by the usage of (4) and its derivative

$$\dot{v} = \dot{H}(x, \dot{x})\dot{x} + H(x)\ddot{x} \quad (19)$$

and substituting them with (10) into (1), resulting in the following equations of motion:

$$\begin{aligned} M(x)H(x)\ddot{x} + \left(M(x)\dot{H}(x, \dot{x}) + C(x, \dot{x})H(x) \right) \dot{x} + G \\ = J^{-T}(x)F_{act}. \end{aligned} \quad (20)$$

The desired trajectory is supposed to be specified by x_{ref} and its derivatives \dot{x}_{ref} and \ddot{x}_{ref} . Hence, the linearizing actuator forces $F_{act, lin}$ can be determined via (20) according to the desired acceleration \ddot{x}_{ref} and, in terms of feedback linearization via the usage of estimation techniques, the estimated \hat{x} and $\dot{\hat{x}}$ as follows:

$$\begin{aligned} F_{act, lin} = J^T(\hat{x})(M(\hat{x})H(\hat{x})\ddot{x}_{ref} \\ + (M(\hat{x})\dot{H}(\hat{x}, \dot{\hat{x}}) + C(\hat{x}, \dot{\hat{x}})H(\hat{x}))\dot{\hat{x}} + G). \end{aligned} \quad (21)$$

If the estimated variables \hat{x} and $\dot{\hat{x}}$ are assumed to comply with the current states, the linearized system behavior can be expressed by the following state equations:

$$\begin{bmatrix} \dot{\hat{x}} \\ \ddot{\hat{x}} \end{bmatrix} = \begin{bmatrix} 0 & I_{6 \times 6} \\ 0 & 0 \end{bmatrix} \begin{bmatrix} \hat{x} \\ \dot{\hat{x}} \end{bmatrix} + \begin{bmatrix} 0 \\ I_{6 \times 6} \end{bmatrix} \ddot{x}_{ref}, \quad (22)$$

representing a double integrative behavior for each mechanical DOF and with the linearized state $\xi = [x^T \dot{x}^T]^T$.

The feedback controller can then be designed to result in a second order lag behavior for the closed loop system for each mechanical DOF, $i = 1 \dots 6$, with the natural frequency ω_i and damping D_i . The complying controller matrix $R \in \mathbb{R}^{6 \times 12}$ consists of two diagonal 6×6 matrices and can be determined as follows:

$$R = [\text{diag}(\omega_i^2) \text{diag}(2D_i\omega_i)]. \quad (23)$$

For the target system the following design parameters were chosen:

$$D_i = 1, i = 1 \dots 6$$

$$\omega_i = 314 \text{ rad/s}, i = 1 \dots 6.$$

The observer based exact feedback linearization and state feedback control can be combined so as to result in a so-called two-degree-of-freedom (2 DOF) control structure as pictured in Fig. 2. Here, the desired \ddot{x}_{ref} is fed forward to ensure a suitable tracking performance, while a state feedback path compensates for model inaccuracies and disturbances. The input for the feedback matrix complies with the difference between the linearized reference state $\xi_{ref} = [x_{ref}^T \dot{x}_{ref}^T]^T$ delayed according to the expected

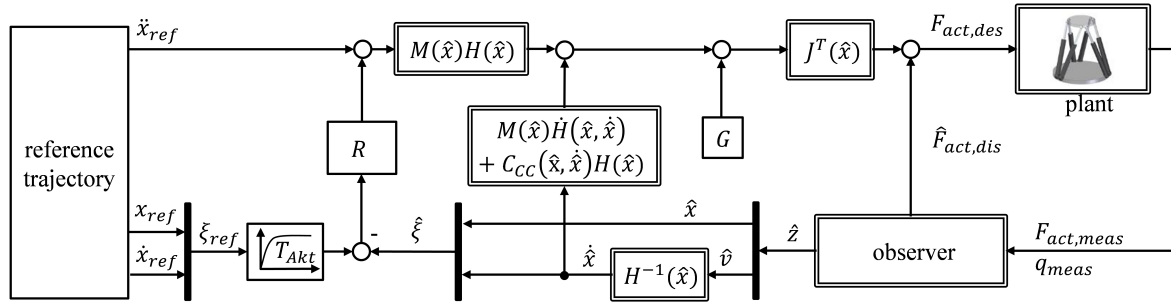


Fig. 2. Control scheme

actuator dynamics, which has also been suggested similarly by Kolbus et al. [2010], and the estimated linearized state $\hat{\xi}_{ref}$. The entire controller output u_C can then be determined using (21), resulting in

$$u_C = J^T(\hat{x}) \left(M(\hat{x})H(\hat{x})(\ddot{x}_{ref} + R(\xi_{ref} - \hat{\xi})) \right. \\ \left. + (M(\hat{x})\dot{H}(\hat{x}, \dot{\hat{x}}) + C(\hat{x}, \dot{\hat{x}})H(\hat{x}))\dot{\hat{x}} + G \right). \quad (24)$$

The estimated linearized state $\hat{\xi}$ can be computed from the estimated state \hat{z} by means of (4). Moreover, if the observer also provides for disturbance estimation, the estimated disturbing forces $\hat{F}_{act,dis}$ can be compensated for via addition to the controller output u_C . If the actuators are assumed to be force controlled, the desired actuator forces $F_{act,des}$ can be determined via

$$F_{act,des} = u_C + \hat{F}_{act,dis}. \quad (25)$$

The generation of \hat{z} and $\hat{F}_{act,dis}$ via nonlinear estimation techniques from the measured joint forces $F_{act,meas}$ and coordinates q_{meas} is treated subsequently.

4. STATE AND DISTURBANCE ESTIMATION

As mentioned above, the current states and disturbances for the usage within the proposed state control strategy shall be generated by means of estimation techniques based on q_{meas} and F_{meas} . Subsequently, a novel approach for the application of sliding mode techniques for this purpose is introduced and its realization for the target system is described. Afterwards, a more classical estimation approach based on Kalman filtering is presented.

4.1 Sliding Mode Observer Preliminaries

Generally, sliding mode algorithms are mainly associated with sliding mode controllers, belonging to robust control systems. Their major disadvantage consists of the chattering effect causing high mechanical stress within the actuators due to the fast switching signals. However, sliding mode techniques can also be applied for estimation purposes where this decisive problem does not occur, as the discontinuous function only impacts on the numerical computation, cf. Spurgeon [2008]. Further advantages of sliding mode observers are the reduced order of the observer dynamics during sliding motion and their robustness against model and parameter uncertainties. Moreover, the possibility of using the equivalent or “average” value of the discontinuous observer feedback signal, which will be explained later, allows to obtain helpful information, e.g.

for fault reconstruction or disturbance rejection (Spurgeon [2008]). In literature, various observer structures for different classes of systems can be found. In Spurgeon [2008] the authors give an overall summary on sliding mode observation and their key properties. Extensive information about general sliding mode algorithms, especially for sliding mode control, and other aspects like chattering can be found in Utkin [1992], Utkin et al. [1999] and Perruquetti et al. [2002].

The here concerned observer structure is often referred to as a hierarchical sliding mode observer. Such kind of observers were first suggested in Drakunov [1992] and they need the afore mentioned equivalent values explicitly to establish sliding motion. In Drakunov et al. [2011] an extended observer structure to Drakunov [1992] was proposed, which also considers system inputs and plant disturbances. The main advantage of such observers is that the design can be accomplished in original system states and a nonlinear state transformation is not required, which usually has to be performed in order to realize common sliding mode observer approaches. As stated in Drakunov et al. [2011], the conditions of applicability for a nonlinear state transformation are more restrictive than observability conditions, e.g. of local observability, which have to be considered for the design of the hierarchical observer. In fact, this issue is a restriction for PKMs, because a state transformation would lead to a system description with joint space coordinates as system states, which is indeed undesirable. A further advantage is that the equivalent feedback values can easily be used to obtain additional information out of the system for disturbance identification.

In the following the basic notion of a hierarchical sliding mode observer is briefly presented. According to Drakunov et al. [2011], the concept is demonstrated for nonlinear control affine systems, cf. (11)-(12), but with a single output, i.e. $p = 1$. In Section 4.2 the observer equations are extended to be used for systems with multiple outputs and hence for the usage within the proposed control scheme for PKMs.

Firstly, a vector function is defined with

$$\Phi(z) = [h_1(z) \dots h_n(z)]^T, \quad (26)$$

where $h_1(z) = h(z)$ is the output equation, cf. (12), and

$$h_i(z) = \frac{\partial h_{i-1}(z)}{\partial z} f(z) = L_f^{i-1} h(z), \quad i = 2, \dots, n, \quad (27)$$

are Lie derivatives of $h(z)$ along $f(z)$. For systems where the relative degree corresponds with the number of system states, the Lie derivatives correspond to:

$$h_i(z) = \dot{h}_{i-1}(z), \quad i = 2, \dots, n. \quad (28)$$

Deriving $\Phi(z)$ by the state vector z , the observability matrix is obtained with:

$$Q(z) = \frac{\partial \Phi(z)}{\partial z}. \quad (29)$$

As stated in Drakunov et al. [2011], the observer can be applied for systems satisfying following condition:

$$\frac{\partial}{\partial z} (Q(z) g(z)) = 0. \quad (30)$$

The hierarchical observer for a nonlinear control affine system with a single output is then given by

$$\dot{\hat{z}} = f(\hat{z}) + g(\hat{z})u + Q^{-1}(\hat{z})\rho(\hat{z})\text{sign}(V(t)). \quad (31)$$

The matrix $\rho(\hat{z})$ represents the observer gains and contains positive diagonal entries as follows

$$\rho(\hat{z}) = \text{diag}(\rho_1(\hat{z}) \dots \rho_n(\hat{z})). \quad (32)$$

The sign function for vector arguments is defined as:

$$\text{sign}(V(t)) = [\text{sign}(\nu_1(t)) \dots \text{sign}(\nu_n(t))]^T, \quad (33)$$

where $V(t) = [\nu_1(t) \dots \nu_n(t)]^T$.

As mentioned in Drakunov [1992], with a suitable choice of the individual $\rho_i(\hat{z})$ sliding modes take place on the respective sliding function $\nu_i(t) = 0$ and after finite time the estimation error converges identical to zero, i.e. $\hat{z}(t) \equiv z(t)$. In general, to provide a sliding motion on, e.g., $s(t) = 0$ the content of the sign function has to correspond to that sliding function, i.e. $\text{sign}(s(t))$. At the hierarchical observer, the first sliding motion takes place on the sliding function $\nu_1(t) = 0$, which contains the difference of the output quantities, with $\nu_1(t) = y(t) - h(\hat{z})$. The subsequent entries of $V(t)$ are:

$$\nu_{i+1}(t) = \{\rho_i(\hat{z})\text{sign}(\nu_i(t))\}_{eq}, \quad i = 1, \dots, n-1. \quad (34)$$

The operator $\{\dots\}_{eq}$ represents an equivalent value of the discontinuous function during sliding motion. According to Utkin et al. [1999] and Spurgeon [2008], this notion can be briefly explained as follows: After an estimation error trajectory, e.g. $\nu_1(t)$, reaches its respective sliding function, e.g. $\nu_1(t) = 0$, the discontinuous feedback signal switches theoretically with infinite frequency, which is indeed a certain idealization. In reality, due to imperfections and delays in every system, the trajectory remains in a small region along the sliding path, whereas the feedback signal switches with finite frequency. These oscillations consist of high and low frequency components. However, the slow components are decisive for the dynamics during sliding motion. After removing the high frequency components out of the injection, e.g. by applying an appropriate low-pass filter, a continuous equivalent value can be obtained. In the field of sliding mode control the approach of deriving the equivalent value is well known as equivalent control method. For the observer in (31) the equivalent values characterize a discrepancy between the plant and the observer model, which can be used to identify disturbances in the plant.

4.2 Sliding Mode Observer Design

By including minor modifications and assumptions, the hierarchical observer concept from Drakunov et al. [2011], which was introduced in Section 4.1, can be applied to the nonlinear control affine system equations of the hexapod,

cf. (11)-(18). In order to begin with the observer design, two considerations need to be taken into account. Firstly, the observer in (31) can only be implemented directly for systems with a single output. However, the considered system has six outputs, the position measurements of the actuators. Therefore, we have to define an appropriate observability matrix $Q(z)$ and show that sliding mode can occur, which allows convergence of the estimation error. Secondly, we have to consider the influence of the system input on the convergence, even though the condition (30) cannot be fulfilled.

Regarding the first point, some ideas and assumptions presented in Chen et al. [2013] can be adapted for the target system. There, the authors performed a nonlinear state transformation to design an asymptotic observer for a hexapod. It can be shown that the relative degree for each output is two and thus the relative degree for the whole nonlinear system is twelve. Hence, for deriving the observability matrix for the system in (11)-(18) the output quantities and their first order derivative are required. They are put together in

$$\Phi(z) = \begin{bmatrix} q(x) \\ \dot{q}(z) \end{bmatrix} = \begin{bmatrix} q(x) \\ J^{-1}(x) \cdot v \end{bmatrix}. \quad (35)$$

The Jacobian of the vector function yields the observability matrix $Q(z) \in \mathbb{R}^{12 \times 12}$, cf. (29):

$$Q(z) = \frac{\partial \Phi(z)}{\partial z} = \begin{bmatrix} J^{-1}(x)H(x) & 0 \\ \frac{\partial(J^{-1}(x) \cdot v)}{\partial x} & J^{-1}(x) \end{bmatrix}. \quad (36)$$

Because of the block matrix structure and the regularity of $J(x)$ and $H(x)$ for the effective workspace of the target system, $Q(z)$ has full rank and the inverse can be calculated with

$$Q^{-1}(z) = \begin{bmatrix} H^{-1}(x)J(x) & 0 \\ -J(x)\frac{\partial(J^{-1}(x) \cdot v)}{\partial x} & H^{-1}(x)J(x) \end{bmatrix} J(x). \quad (37)$$

Due to the fact that the observability matrix is invertible it follows that the nonlinear system is locally observable, see Hermann et al. [1977].

The matrix with the observer gains $\rho(\hat{z})$ is selected as follows:

$$\rho(\hat{z}) = \rho = \begin{bmatrix} \rho_1 \cdot I & 0 \\ 0 & \rho_2 \cdot I \end{bmatrix}, \quad (38)$$

where I is a 6×6 identity matrix. Since the values are gains for similar sign functions, the first six and secondary six diagonal entries can be chosen equally. Also it turned out that constant gains are sufficient to guarantee convergence of the observer. The vector of estimated states consists of the estimated position vector \hat{x} and the estimated velocity vector \hat{v} , with $\hat{z} = [\hat{x}^T \hat{v}^T]^T$. In the following the difference of the measured and observed outputs is denoted with $e_q(t) = q_{meas}(t) - q(\hat{x})$.

The matrix $V(t)$, which includes the output differences and the equivalent values, consists of two vectors $\nu_1(t) \in \mathbb{R}^6$ and $\nu_2(t) \in \mathbb{R}^6$, with

$$V(t) = \begin{bmatrix} \nu_1(t) \\ \nu_2(t) \end{bmatrix} = \begin{bmatrix} e_q(t) \\ \{\rho_1 \text{sign}(e_q(t))\}_{eq} \end{bmatrix}. \quad (39)$$

Finally, the suggested observer for the PKM has the same structure as in (31) but consists of suitable matrices, cf.

(35)-(39), and u corresponds to F_{meas} . In our case the condition in (30) can not be satisfied, because

$$Q(z)g(z) = \begin{bmatrix} 0 \\ J^{-1}(x)M^{-1}(x)J^{-T}(x) \end{bmatrix}, \quad (40)$$

depends on x . However, it can be shown that the proposed observer still converges. The key facts are that the first six rows of (40) are zero and the matrix is nearly constant in the considered workspace of the target system. Additionally, the input appears only in the last six estimation error equations, which can be seen in the following.

The feasibility of the proposed observer can be demonstrated by means of the convergence proof from Drakunov [1992]. There it is shown that convergence of the estimated outputs and their repeated derivatives represents convergence of the estimated states. Indeed, this is the case if the Jacobian of the map $\Phi(z)$, cf. (35), is regular. For convergence analysis the time derivative of the estimation error $e_\Phi = (\Phi(z) - \Phi(\hat{z}))$ is relevant:

$$\begin{aligned} \dot{e}_\Phi &= \frac{d}{dt}(\Phi(z) - \Phi(\hat{z})) = Q(z)\dot{z} - Q(\hat{z})\dot{\hat{z}} \\ &= Q(z)(f(z) + g(z)u) \\ &\quad - Q(\hat{z})(f(\hat{z}) + g(\hat{z})u) - \rho \text{sign}(V(t)). \end{aligned} \quad (41)$$

Firstly, the first six rows of the differential equation are investigated. Since $e_\Phi = [e_q^T \ e_q^{T_1}]^T$, the first vector of e_Φ corresponds to the estimation error of the outputs and accordingly of the actuator lengths. By means of (16) and (17) the time derivative yields:

$$\dot{e}_q = J^{-1}(x)v - J^{-1}(\hat{x})\hat{v} - \rho_1 \text{sign}(e_q). \quad (42)$$

In (42) it can be seen that for sufficiently large ρ_1 , in particular $\rho_1 \geq \max |J^{-1}(x)v - J^{-1}(\hat{x})\hat{v}|$, sliding mode occurs on $e_q = 0$. During sliding motion the equivalent value is given by $\nu_2 = \{\rho_1 \text{sign}(e_q)\}_{e_q} = J^{-1}(x)v - J^{-1}(\hat{x})\hat{v}$. According to (8), the equivalent value ν_2 corresponds to the difference of the actuator velocities $e_{\dot{q}}$.

For sake of simplicity, we will not write down the error equations for the second part of (41). After some matrix multiplications it results a structure similar to (42). The error equation can be expressed with

$$\dot{e}_{\dot{q}} = \ddot{q}(z, u) - \ddot{q}(z, u)|_{z=\hat{z}} - \rho_2 \text{sign}(e_{\dot{q}}), \quad (43)$$

where $\ddot{q}(z, u)$ and $\ddot{q}(z, u)|_{z=\hat{z}}$ represent the real and estimated actuator accelerations. And again, for sufficiently large ρ_2 sliding mode takes place on the function $e_{\dot{q}} = 0$. In a first approximation the concrete values for the individual ρ_i can be obtained by considering the initial conditions. As shown above, sliding mode will occur successively and in two steps the output estimation error will converge, which leads to successful state estimation.

In the following, it is demonstrated how a mismatch between the plant and observer can be identified just by using the equivalent values. Here, we assume that a disturbance $\phi(t)$, which is bounded, will appear in the last error functions in (43), e.g. caused by unknown forces and and torques in the plant. As mentioned above, the observer will converge for sufficiently large ρ_2 , even if disturbances exist. After the observer has reached the second sliding function $e_{\dot{q}} = 0$, the equivalent observer feedback corresponds to:

$$\{\rho_2 \text{sign}(e_{\dot{q}})\}_{e_{\dot{q}}} = \phi(t). \quad (44)$$

In order to obtain the disturbances $\phi(t)$ simply the high frequency components of the discontinuous function in (43) have to be filtered out. Then, the disturbing forces and momentums at the center of mass of the end effector in N , denoted by $s(t) = [s_1(t) \dots s_\eta(t)]^T$, can be calculated with:

$$s(t) = M(\hat{x})J(\hat{x})\phi(t). \quad (45)$$

Here, instead of using low pass filters to avoid additional delays in the observer, an alternative approach is applied. According to Tan et al. [2003], the equivalent observer feedback signals can be approximated, e.g. for the first component of vector ν_2 in (39), with:

$$\nu_{2,1} = \{\rho_1 \text{sign}(e_{q,1})\}_{e_q} \approx \rho_1 \frac{e_{q,1}}{|e_{q,1}| + \delta}, \quad (46)$$

where δ is a small positive constant, characterizing the accuracy of the equivalent values. Additionally, chattering reduction is accomplished by using this approximation of the discontinuous functions. For details and restrictions see Tan et al. [2003] and the references therein.

4.3 Continuous State and Disturbance Estimation

The subsequently presented estimation approach bases upon the one we already presented in Flottmeier et al. [2013]. Here, the Kalman-Bucy filter is extended by a disturbance estimation part. The complying observer equations are given by

$$\dot{\hat{z}}_d = f_d(\hat{z}_d) + g_d(\hat{z}_d)u + K(y - \hat{y}_d) \quad (47)$$

$$\hat{y}_d = h(\hat{z}_d). \quad (48)$$

Here, u corresponds to F_{meas} and y to q_{meas} . The vector $\hat{z}_d \in \mathbb{R}^{18}$ represents the observer state vector with

$$\hat{z}_d = [\hat{x}^T \ \hat{v}^T \ \hat{s}^T]^T, \quad (49)$$

where $s^T = [s_1 \dots s_6]^T$ represents the vector of disturbing forces and torques acting at the center of mass of the end effector in N . The dynamic behavior of s is assumed to be characterized by the following differential equation:

$$\dot{s} = 0. \quad (50)$$

Accordingly, $f_d(\hat{z}_d)$ and $g_d(\hat{z}_d)$ can be generated by extension of (16) and (17), resulting in

$$\begin{aligned} f_d(\hat{z}_d) &= \begin{bmatrix} 0 & H^{-1}(\hat{x}) & 0 \\ 0 & -M^{-1}(\hat{x})C(\hat{x}, \hat{v}) & M^{-1}(\hat{x}) \\ 0 & 0 & 0 \end{bmatrix} \hat{z}_d \\ &\quad + \begin{bmatrix} 0 \\ -M^{-1}(\hat{x})G \\ 0 \end{bmatrix}, \end{aligned} \quad (51)$$

$$g(\hat{z}_d) = \begin{bmatrix} 0 \\ M^{-1}(\hat{x})J^{-T}(\hat{x}) \\ 0 \end{bmatrix}, \quad (52)$$

$$h(\hat{z}_d) = q(\hat{x}). \quad (53)$$

The design of the observer gain matrix $K \in \mathbb{R}^{6 \times 18}$ bases upon a linearized system representation, which is used to solve the algebraic Riccati equation

$$PC_{lin}^T S_{KF}^{-1} C_{lin} P - PA_{lin}^T - A_{lin} P - Q_{KF} = 0. \quad (54)$$

The required linearized system matrices A_{lin} and C_{lin} can be calculated from (47) and (48) by a Taylor series truncated after the first term:

$$A_{lin} = \left. \frac{\partial \dot{\hat{z}}_d}{\partial \hat{z}_d} \right|_{\hat{z}_{d,0}, u_0} \quad C_{lin} = \left. \frac{\partial \hat{y}_d}{\partial \hat{z}_d} \right|_{\hat{z}_{d,0}} \quad (55)$$

Table 2. Plant model properties

6 DOF model	
end effector platform mass	217 kg
MBS model	
end effector platform mass	169 kg
effective piston area	742 mm ²
mass of one piston rod	8 kg
nominal flow rate	38 l/min
nominal pressure drop (per control edge)	35 bar
servo valve cut-off frequency	350 Hz
supply pressure	280 bar

with $\hat{z}_{d,0} = [\hat{x}_0^T \ 0^T \ 0^T]^T$, \hat{x}_0 located in the center of the workspace and $u_0 = J^T(\hat{x}_0)G$. The weighting matrices define the trade-off between confidence in model accuracy (Q_{KF}) and measurement data (S_{KF}).

Actually, due to the system's nonlinearities it would be intuitive to apply an Extended Kalman filter. However, the effective workspace of the hexapod is limited due to the mechanical boundary conditions. In Flottmeier et al. [2013] it was shown by the analysis of eigenvalues that the usage of a constant K does not lead to instabilities for the pure state estimation task. This can be shown for the extension of the Kalman filter by disturbance estimation, too.

For the usage within the above presented state control scheme, \hat{s} can be transferred to $\hat{F}_{act,dis}$ via

$$\hat{F}_{act,dis} = J^T(\hat{x}) \cdot \hat{s}. \quad (56)$$

5. ANALYSIS

The effectiveness of the presented estimation approaches was evaluated via simulations with plant models of different complexity. At first, simulations with a six DOF model were carried out to proof the general functionality and allow a first comparison of the estimation performance. Here, the difference between the observer and plant model only consisted of the additional consideration of actuator dynamics and Coulomb friction forces within the plant model. Secondly, a complex MBS model with 13 masses and considering the nonlinearities due to the hydraulic actuation was used to test the control and estimation performance more realistically. The geometric parameters of the plant models correspond to the ones given in Table 1; additional properties are listed in Table 2.

5.1 Simulation Results with Six DOF Plant Model

Simulations with the six DOF plant model were carried out using continuous reference variables representing a sinusoidal movement of the TCP with 1 cm amplitude and a frequency of 10 Hz in the x -direction of N . In order to prevent discontinuities at the beginning of the movement, the reference variables were filtered by a second order lag element with a cut-off frequency of 80 Hz. The x -direction represents a poorly actuated DOF, hence movements in this direction allow a suitable analysis of the control and estimation performance in terms of decoupling.

At first, simulation data was generated to investigate the general state estimation performance of the Kalman filter (KF) and sliding mode observer (SM) without disturbance

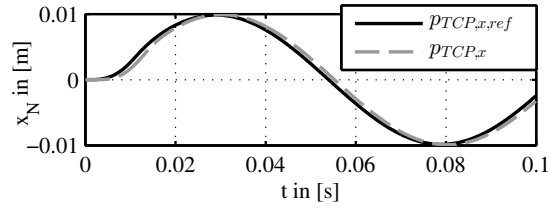


Fig. 3. Reference variable and system response in x -direction

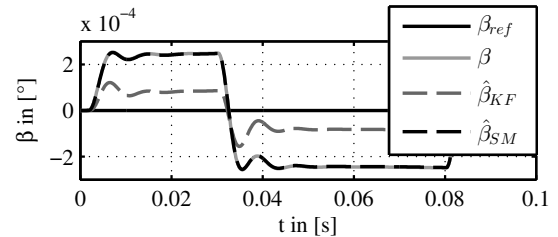


Fig. 4. Reference variable, system response and estimated system response in β -direction

estimation and control impacts. In order to achieve this, the plant state was used for feedback purposes instead of the estimated state (this setup will be called *ideal control* subsequently) and disturbances were not compensated for. Fig. 3 shows the corresponding response for the above mentioned excitation in the x -direction. Here no major differences between the real and estimated variables occur, the deviations are within a range of 10^{-6} m. Therefore, the estimated variables are not shown.

This is different for the movement around the y -axis (in the β -direction), which is highly coupled to the one in the x -direction due to the kinematic structure, cf. Fig. 1. The complying results are shown in Fig. 4. Here, the reference variable is actually zero, while deviations in the system behaviour and the estimated behavior occur. The bad control tracking behavior results from the Coulomb friction forces, not having been considered explicitly within the control design. It can be observed that the overall estimation performance of the sliding mode observer ($\hat{\beta}_{SM}$) is clearly better than the one of the Kalman filter ($\hat{\beta}_{KF}$), as its curve exactly lies on top of the one of the simulated system response. Hence, it seems to be more robust in terms of input disturbances. Consequently, if the estimated states of the sliding mode observer are used for control purposes (still without disturbance compensation), the tracking performance is almost the same as for the control with the ideal states and clearly better compared to the control based on the states estimated by the Kalman filter, which is shown in Fig. 5.

The presented estimation approaches also allow for disturbance estimation. In order to investigate this, the Coulomb friction forces of 85 N having been considered within the plant model can be used. They should be identified appropriately, as they represent the major difference between plant and observer model. In Fig. 6 the complying simulation results are shown. As it can be seen, the friction forces are estimated correctly by both observers, while the Kalman filter is slightly slower and shows a small overshoot.

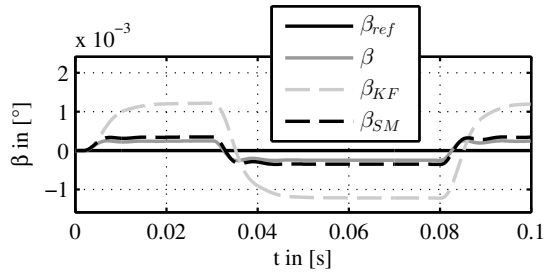


Fig. 5. System response in β -direction for ideal and observer based control without disturbance estimation

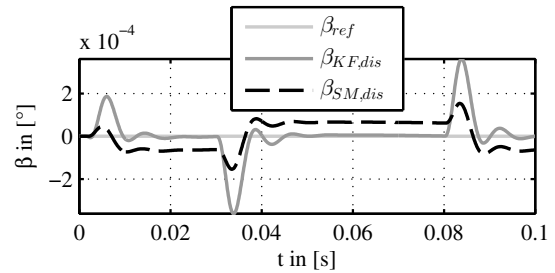


Fig. 8. System response in β direction for observer based control with disturbance compensation

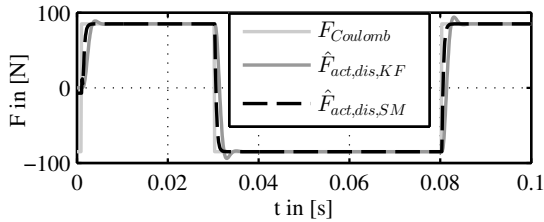


Fig. 6. Disturbances

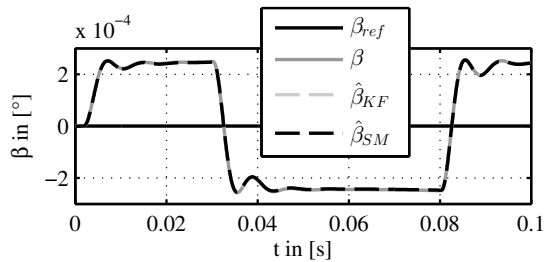


Fig. 7. System response and estimated system responses for observation with disturbance estimation

However, the consideration of disturbances within the Kalman filter also leads to better state estimation performance for this estimation approach. This can be seen in Fig. 7, where the estimated states are shown for control based on the ideal state and without disturbance compensation, again (the same experiment as in Fig. 4, but with disturbance estimation). The estimator curves lay on top of the system response, so now the state estimation performance of the Kalman filter is as good as the one of the sliding mode observer.

Finally, the overall control performance for the realization of the entire control scheme with disturbance compensation as pictured in Section 3 is analyzed for both estimation approaches. Fig. 8 shows the complying system behavior, again in β -direction. The tracking performance is clearly better than the one for the ideal state feedback, cf. Fig. 4, or the one for the observer based control without disturbance estimation and compensation, cf. Fig. 5. In comparison, the controlled system based on Kalman filter estimation shows higher oscillations, while the one based on sliding mode estimation has a small steady state error. As for the Kalman filter, this can be assumed to result from the overshoot in the disturbance estimation that impacts the system behaviour via the disturbance compensation. In terms of the sliding mode observer, the small steady state error may result from the fact that there is no feedback from the estimated disturbances to the state estimation.

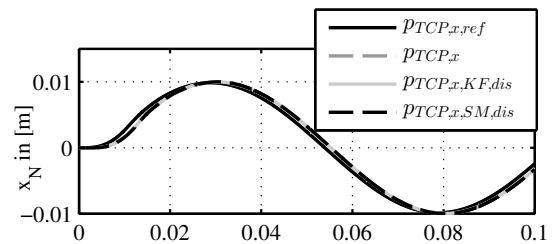
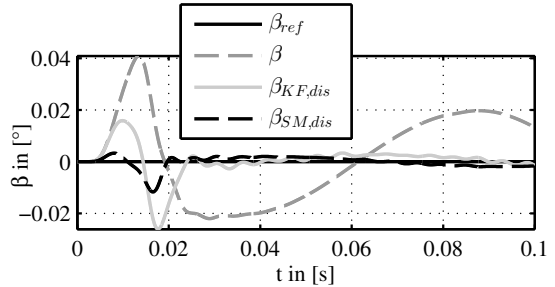


Fig. 9. System response for ideal and observer based control with disturbance compensation and MBS plant model



5.2 Simulation Results with MBS Plant Model

In a second step, the suitability of the estimation approaches within the advanced state control structure was evaluated by means of simulations with a complex MBS plant model, also considering the nonlinearities due to the hydraulic actuation. The MBS model consists of 13 masses, so it also allows the evaluation of the control performance considering model inaccuracies, as it clearly differs from the six DOF model that has been used for the control and observer design. The single actuators were modeled to be locally force controlled by a suitable nonlinear control approach according to Rost et al. [2012]. The reference variables were chosen just like the ones used in Section 5.1.

The reference variables and the complying system responses for ideal and observer based control are shown in Fig. 9. Again, the control performance of the observer based control with disturbances compensation is clearly better than the one of the ideal control without disturbance compensation. Moreover, the control with the Kalman filter shows higher oscillations than the one with the sliding mode observer, again. However, differences concerning the steady state error that occurred previously (cf. Fig. 8) cannot be recognized.

The differences between the plant and the model used for control and observer design do not lead to major deviations or instabilities. Hence, the proposed state control scheme and both estimation approaches for its realization are assumed to be suitable for the usage within the planned application. However, differences in the control performance occur and leave open questions to be answered in the future.

6. FUTURE OUTLOOK

The characteristics of the presented estimation approaches still have to be further investigated. One aspect to be analyzed is the fact that disturbances, which are estimated from the measured actuator forces and displacements, can be estimated very fast according to the observer dynamics. However, if they shall be compensated for, the actuator dynamics limit the bandwidth of the disturbance compensation. Hence, this could lead to instabilities and probably has to be treated by the usage of some kind of anti aliasing filter.

A second aspect to be investigated is the impact of the fact that the sliding mode observer model is of second order, while the model used for the Kalman filter with disturbance estimation is of third order. This has to be regarded in terms of realtime application, as it can be assumed to influence the required integration stepsize and computational effort.

The potential of the sliding mode estimation approach has not been fully examined and exploited, yet. It will be analyzed considering the impact of noisy measurement signals. Additionally, the application of super twisting algorithms (STA), which base on second order sliding mode techniques, will be examined in order to enhance performance of the estimation.

The above presented control approach will be further investigated in terms of the impact of limitations due to the hydraulic actuation. Finally, the entire control structure will be tested at the target system, which is currently build up at the Heinz Nixdorf Institute of the University of Paderborn.

REFERENCES

- H. Abdellatif and B. Heimann. Passivity-Based Observer/Controller Design with Desired Dynamics Compensation for 6 DOFs Parallel Manipulators. In *Proceedings of the 2008 IEEE/RSJ International Conference on Intelligent Robots and Systems*, Nice, France, 2008.
- S.-H. Chen and L.-C. Fu. Output Feedback Sliding Mode Control for a Stewart Platform With a Nonlinear Observer-Based Forward Kinematics Solution. In *IEEE Transactions on Control Systems Technology* 21(2013), pages 176–185.
- S. Drakunov. Sliding-Mode Observers Based on Equivalent Control Method. In *Proceedings of the 31st Conference on Decision & Control*, Tucson (Arizona), 1992.
- S. Drakunov and V. Utkin. Sliding Mode Observers. Tutorial. In: *Proceedings of the 34th Conference on Decision & Control*, New Orleans (LA), 1995
- S. Drakunov and M. Reyhanoglu. Hierarchical sliding mode observers for distributed parameter systems. In: *Journal of Vibration and Control*, 17(10), pages 1441–1453, 2011.
- E. D. Fasse and A. J. Wavering. Configuration Estimation of Gough-Stewart Platforms Using Extended Kalman Filtering. In: *Proceedings of DETC'00 ASME 2000 Design Engineering Technical Conferences and Computers and Information in Engineering Conferences*, Baltimore, USA, 2000.
- S. Flottmeier and A. Trächtler. 2-DOF State Control Scheme for the Motion Control of a Parallel Kinematic Machine. In: *Proceedings of the 2nd International Conference on Control and Fault-Tolerant Systems*, Nice, France, 2013.
- L. Fraguera, L. Fridman and V. V. Alexandrov. Position stabilization of a Stewart platform: High-order sliding mode observers based approach. In: *Journal of the Franklin Institute* 349(2), pages 441–455, 2012.
- R. Hermann and A. J. Krener. Nonlinear Controllability and Observability. In: *IEEE Transactions on Automatic Control* 22(05), pages 728–470, 1977.
- J.-Y. Kang, D. H. Kim and K.-I. Lee. Robust Estimator Design for Forward Kinematics Solution of a Stewart Platform. In *Journal of Robotic Systems* 15(1), pages 29–42, 1998.
- M. Kolbus, F. Wobbe, T. Reisinger and W. Schumacher. Integrated Force and Motion Control of Parallel Robots - Part 1: Unconstrained Space. In: D. Schütz and F. Wahl (eds.) *Robotic systems for handling and assembly* Vol. 67. Springer, Berlin Heidelberg, 2010.
- J.-P. Merlet. Still a long way to go on the road for parallel mechanisms. *ASME 2002 DETC Conference*, Montréal, 2002.
- J.-P. Merlet. *Solid mechanics and its applications*. Vol. 128: *Parallel Robots*. 2nd ed., Dordrecht and the Netherlands, Springer, 2006.
- F. Paccot, N. Andreff, P. Martinet. A Review on the Dynamic Control of Parallel Kinematic Machines: Theory and Experiments. In: *The International Journal of Robotics Research* 28(1), pages 395–416, 2009.
- W. Perruquetti and J. P. Barbot. Sliding Mode Control in Engineering. Marcel Dekker, 2002.
- R. E. Roberson and R. Schwertassek. Dynamics of Multi-body Systems. Springer-Verlag Berlin Heidelberg, 1988.
- S. Rost, V. Sklyarenko, F. Schreiber and W. Schumacher. Design of a Modular Hydraulically Driven Variable Geometry Truss Structure and its Nonlinear Controller Architecture of Highly Dexterous Motion. In: *Proceedings of the 8th International Fluid Power Conference*, Dresden, 2012
- S. K. Spurgeon. Sliding mode observers: a survey. In *International Journal of Systems Science* 39:8, pages 751–764, 2008.
- C. P. Tan and C. Edwards. Sliding mode observers for reconstruction of simultaneous actuator and sensor faults. In: *Proceedings of the 42nd IEEE Conference on Decision & Control*, Maui (Hawaii), 2003
- V. Utkin, J. Guldner and J. Shi. Sliding Mode Control in Electromechanical Systems. CRC Press, 1999.
- V. Utkin. Sliding Modes in Control Optimization. Springer Verlag, 1992.